Available online at www.sciencedirect.com
SCIENCE DIRECT
Journal of Catalysis 242 (2006) 217–226
JOURNAL OF CATALYSIS
www.elsevier.com/locate/jcat

Improving the coking resistance of Ni-based catalysts by promotion with subsurface boron

Jing Xu, Mark Saeys *

Department of Chemical and Biomolecular Engineering, 4 Engineering Drive 4, National University of Singapore, Singapore 117576

Received 27 April 2006; revised 31 May 2006; accepted 31 May 2006

Abstract

Carbon deposition on Ni catalysts was analyzed using first-principles density functional theory calculations. Based on the analysis, we propose boron as a promoter to improve the coking resistance of Ni-based catalysts. Three types of chemisorbed carbon were identified: on-surface carbon atoms, bulk carbon atoms, and extended graphene islands. Extended graphene islands were calculated to be the thermodynamically most stable form of deposited carbon. However, the formation of graphene islands requires high carbon surface coverage and might be kinetically limited at lower carbon coverage. Bulk carbon is found to be more stable than on-surface carbon and can form readily, even at low carbon coverage. Both bulk carbon and graphene islands might lead to catalyst deactivation and should be prevented. Addition of small amounts of boron to the Ni catalyst was found to inhibit the formation of bulk carbide and weaken the on-surface carbon binding energies, possibly slowing the formation of graphene islands. According to our calculations, boron prefers to adsorb in the octahedral sites just below the surface, rather than in the Ni bulk. A small amount of boron corresponding to a single monolayer was found to be sufficient to reduce coking of Ni-based catalysts.

Keywords: Carbon chemisorption; Coking; Ni catalysts; Density functional theory; Boron promoter

1. Introduction

Ni-based catalysts are widely used in such chemical processes as hydrogenation and dehydrogenation, stream reforming, and catalytic partial oxidation (CPO) of natural gas [1,2]. As a transition metal, Ni-based catalysts exhibit high activity for these reactions and are cost-effective in comparison with Pt-, Ru-, Rh-, or Pd-based catalysts. However, catalyst deactivation by carbon deposition, commonly termed "coking," is a general problem for hydrocarbon reactions over such transition metal catalysts as Fe, Co, and Ni [3,4]. Carbon deposition on the catalyst might cause loss of active sites, whereas growth of filamentous carbon nanotubes can lead to reactor blocking. Catalyst deactivation is especially problematic for Ni-based catalyst [5,6]. Indeed, Ni is commonly used as a catalyst to grow carbon nanotubes because of its rapid carbon deposition rates [7]. Noble metal catalysts, such as Rh and Ru, show much higher coking resistance [8], but they significantly increase catalyst cost. Improving the coking resistance of Ni-based catalysts has the potential to greatly enhance the run time of a number of important chemical processes and has been an area of intensive research. As a result, different promoters have been proposed to improve the coking resistance of Ni-based catalysts [9,10].

Coking of Ni surfaces is an important technological problem, and a number of experimental studies have addressed this process [11–19]. The main pathways leading to carbon atoms on the catalyst surface are the catalytic dehydrogenation of hydrocarbons, $C_mH_n \rightarrow mC + \frac{1}{2}nH_2$, and CO disproportionation via the Boudouard reaction, $2CO \rightarrow C + CO_2$. Hydrocarbon dehydrogenation dominates at high temperatures, whereas the Boudouard reaction is a low-temperature pathway to carbon atoms [12]. At the molecular scale, three types of chemisorbed carbon can be distinguished: (i) isolated on-surface carbon atoms; (ii) a carbide-like structure where carbon atoms are dissolved in the Ni bulk; and (iii) extended islands of graphene, a single sheet of graphite. On-surface carbon atoms are active reaction intermediates that combine with hydrogen in Fischer–Tropsch synthesis or methanation, and with oxygen atoms dur-

* Corresponding author. Fax: +65 6779 1936.
E-mail address: chesm@nus.edu.sg (M. Saeys).

0021-9517/$ – see front matter
doi:10.1016/j.jcat.2006.05.029

ing reforming and partial oxidation. The graphene islands block active sites on the Ni catalyst surface. The carbon atoms in the graphene islands, as well as the bulk carbon atoms, do not participate in the reaction, and their formation should be avoided.

The mechanism of coking of Ni catalysts is closely related the growth of carbon nanotubes on nanoscale Ni particles. The latter process has received considerable recent attention. Generally, a three-step mechanism is observed for the growth of carbon nanotubes on Ni catalysts [13,14], namely, a nucleation step, a growth phase, and finally deactivation of the Ni catalyst by encapsulation. In this mechanism, the first step is the dissociation of hydrocarbon molecules to form adsorbed carbon atoms. The isolated surface carbon atoms are believed to dissolve in the Ni catalyst particle and diffuse from the gas side to the support side via the formation of an intermediate carbide phase [15,16]. This is the nucleation step, which is followed by the growth of carbon nanotubes. The growth of carbon nanotubes terminates by encapsulation of the Ni particles with carbon. Recently, Abild-Pedersen et al. [17] presented a detailed density functional theory (DFT) study of the initial stages in the mechanism of graphene growth from a step-edge on a Ni catalyst. Different transport mechanisms involving surface, subsurface, and bulk carbon diffusion, as well as Ni atom transport from the step edge, were considered. In addition, activation energies were calculated for the addition of carbon atoms to the perimeter of a growing graphene sheet. It was found that the preferred carbon transport mechanism is surface or subsurface diffusion, whereas diffusion through the bulk of the Ni catalyst is associated with a high activation barrier.

The formation of bulk carbide from CO disproportionation and from methane dissociation has been confirmed experimentally. Nakamura et al. [18] studied CO disproportionation over Ni(100) and Ni(111) surfaces and observed the formation of a bulk carbide at 660 K. A scanning tunneling microscopy study of CO disproportionation over a stepped Ni(977) surface confirmed the formation of three to four layers of a bulk Ni carbide at 500 K [19]. Formation of a bulk carbide after methane dissociation on Ni(110) and Ni(100) surfaces was observed experimentally at temperatures above 533 K [20].

Temperature-programmed oxidation has been used to determine the carbon binding energy for Ni catalysts as a function of carbon surface coverage [21]. Three regions of carbon binding energies were observed: high values at around −780 kJ/mol associated with carbon atoms in a graphene structure; intermediate values between −700 and −740 kJ/mol, which the authors assume to correspond to carbon atoms adsorbed at two types of steps on the surface; and relatively low values at around −660 kJ/mol, corresponding to Ni(111) terrace sites.

A number of theoretical studies have been published on the chemisorption of carbon on a Ni(111) surface. Bengaard et al. [22] used DFT to study the influence of potassium, sulfur, and gold on the formation of a graphene overlayer on a Ni(111) surface. Klinke et al. [23] performed calculations for on-surface carbon, subsurface carbon, and graphene chemisorption on a Ni(111) surface to provide insight into the mechanism of Fischer–Tropsch synthesis. The fcc threefold-hollow site was found to be the preferred on-surface adsorption site with a binding energy of −644 kJ/mol. The subsurface octahedral site was found to be preferred over the fcc threefold-hollow site for coverage of 0.25–1.0 ML.

Because deactivation is an important limitation in the application of Ni-based catalysts, various studies have proposed promoters to improve the coking resistance of Ni-based catalysts. An early proposal was to selectively poison the most active sites of the Ni catalyst using sulfur [10]. It was found that trace amounts of adsorbed sulfur poison the graphite formation more than they poison the reforming reaction [24]. Recently, it was found that alloying Ni-based catalysts with small amounts of gold also greatly reduces coking [9,22]. First-principles calculations [22] indicate that a similar principle can explain the increased stability of Ni-based catalysts promoted with small amounts of sulfur, gold, and potassium. All three atoms show a strong preference for adsorption at step sites on the Ni surface. Step sites have been proposed as the nucleation sites for graphene formation [17,22], and hence selectively blocking the step sites greatly improves the resistance of Ni-based catalysts against graphene formation. Recently, Chen et al. [25] demonstrated that boron promotion also can improve the coking resistance of Ni-based catalysts during the catalytic partial oxidation of methane. The coking resistance of Ni-based catalysts with different catalyst loadings but a similar Ni:B atomic ratio of about 85:15 was reported. The authors speculated that the enhanced coking resistance is related to the higher dispersion and the smaller particle size of the NiB catalyst particles. Boron has also been suggested to improve the sulfur poisoning resistance of Co-based catalysts for Fischer–Tropsch synthesis [26]. Adding 0.05 wt% B to a 10 wt% Co catalyst was found to improve the sulfur tolerance of the catalyst. In this paper we use DFT calculations to try to elucidate how adding B influences the coking of Ni-based catalysts.

The paper is structured as follows. First, DFT calculations are performed to gain insight into the thermodynamics and kinetics of carbon deposition on a Ni(111) surface. The stability of the three types of chemisorbed carbon and the kinetics of their interconversion are discussed. Our data expand some of the earlier work by Bengaard et al. [22] and Klinke et al. [23]. Starting from a mechanistic understanding of the coking mechanism, the effect of boron on carbon deposition is discussed. In this paper we focus on the location of the boron atoms and their effect on carbon binding energies for the dominant Ni(111) surface. Based on our first-principles calculations, we propose boron promotion to improve the coking resistance of Ni-based catalysts.

2. Computational methods

Carbon chemisorption energies were calculated using periodic spin-polarized DFT with the Perdew–Wang 91 [27] functional as implemented in the Vienna ab initio simulation package (VASP) [28,29]. The calculations were performed using a plane wave basis, with a cutoff kinetic energy of 400 eV. Projector-augmented wave (PAW) pseudopotentials [30,31] were used to describe the inner shell electrons. Carbon chemisorption energies were calculated for the thermodynam-

ically preferred Ni(111) surface. The Ni catalyst was modeled as a four-layered slab in which the topmost two layers are allowed to relax and the remaining layers are fixed at their bulk positions. Increasing the slab thickness from four to six layers was found to increase the C and B adsorption energies by <2 kJ/mol for monolayer coverages. The optimized bulk lattice constant of 3.52 Å is in good agreement with the experimental value of 3.524 Å [32]. For calculations for subsurface chemisorption of carbon and boron, only the bottom layer was constrained at the bulk positions, because subsurface carbon and boron atoms cause significant interlayer expansion. To calculate the activation energies, the potential energy surface for carbon diffusion from the surface to the subsurface sites was calculated by varying the carbon-to-surface distance in 0.2-Å steps.

Modeling of 0.125, 0.25, 0.33, 0.5, and 1.0 monolayer (ML) coverages was done using $p(4 \times 2)$, $p(2 \times 2)$, $p(\sqrt{3} \times \sqrt{3})$, $p(2 \times 1)$, and $p(1 \times 1)$ unit cells, respectively. An interslab spacing of 12 Å was found to be sufficient to avoid interactions between repeated slabs. Increasing the thickness of the vacuum layer from 12 to 36 Å was found to change the calculated binding energies by <1 kJ/mol. Convergence with respect to k-point sampling was also confirmed for both C/Ni and B/Ni systems. For coverage of <0.25 ML, binding energies converge within 3 kJ/mol when a $(5 \times 5 \times 1)$ Monkhorst–Pack grid is used for the Brillouin-zone integrations. Due to the faster variations in the electron density for a $p(1 \times 1)$ unit cell, a slightly finer $(7 \times 7 \times 1)$ grid is required to reach convergence within 2 kJ/mol.

Binding energies, E_b, were calculated using

$$E_b = 1/N_X(E_{(X/Ni)} - E_{(Ni,clean)} - N_X E_{(X)}), \quad (1)$$

where $E_{(X/Ni)}$, $E_{(Ni,clean)}$, and $E_{(X)}$ represent the total DFT energy of the combined X/Ni (X = C or B) system, the clean surface, and the free atom, respectively, and N_X is the number of carbon or boron atoms per unit cell.

3. Results and discussion

In what follows we propose a mechanism for carbon deposition based on first-principles calculations. First, the thermodynamic stabilities of the various types of chemisorbed carbon are calculated and the kinetics governing their formation discussed. Next, the effect of boron on carbon chemisorption is addressed.

3.1. Thermodynamic diagram for chemisorbed carbon

As highlighted in the Introduction, three types of chemisorbed carbon can be distinguished: on-surface carbon, subsurface or bulk carbon, and graphene islands. We start our discussion with on-surface carbon adsorption. There are four high symmetry adsorption sites on a Ni(111) surface: atop, two-fold bridge, and fcc and hcp threefold-hollow sites. The carbon binding energies at all four sites were calculated for coverages ranging from 0.125 to 1.0 ML and are plotted in Fig. 1. Binding energies at the hcp and fcc hollow sites are fairly similar and preferred

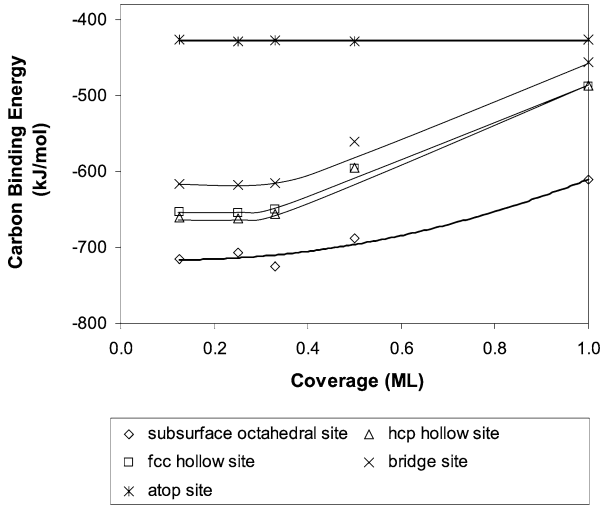

Fig. 1. Carbon binding energies for chemisorption at the four high symmetry sites of the Ni(111) surface and at the octahedral sites of the first subsurface layer as a function of coverage. The symbols indicate the calculated binding energies, the lines are guides for the eye.

over those of the bridge and atop sites. At low coverage, adsorption at the hcp site is slightly stronger (by about 7 kJ/mol) than adsorption at the fcc site. The site preference changes for monolayer coverages, where adsorption is 0.5 kJ/mol stronger at the fcc site than at the hcp site. The binding energy at the hollow sites depends strongly on the carbon coverage, decreasing from −487 kJ/mol at 1.0 ML to −660 kJ/mol at 0.125 ML. Our binding energies are consistent with the values published by Klinke et al. [23] for coverages of 0.25 and 1.0 ML and with experimental values published by Bjørgum et al. [21].

Experimental studies indicate that on-surface carbon atoms spontaneously dissolve into the Ni bulk at sufficiently high temperatures [11,15,33]. To gain insight into the location and the distribution of these bulk carbon atoms, binding energies were calculated for carbon atoms in the first and second subsurface layers and in the Ni bulk. Carbon chemisorption at the octahedral sites of the first subsurface layer is preferred over on-surface chemisorption for all coverages studied (Fig. 1). On subsurface carbon chemisorption, the Ni–Ni interlayer spacing increases significantly, for example, from 2.01 to 2.36 Å for a concentration equivalent to 0.5 ML. In addition, the lattice constant for Ni slab increases slightly in the calculations, for example, from 3.52 to 3.55 Å for a concentration corresponding to 0.5 ML. Carbon binding energies in the first subsurface layer are less coverage-dependent than on-surface binding energies. For low coverage, subsurface chemisorption was about 50 kJ/mol more stable than on-surface chemisorption; this preference increases to 120 kJ/mol for monolayer coverage. The calculations indicate that there is a driving force for carbon atoms to diffuse into the Ni bulk, consistent with experimental observations. The preference of carbon atoms for subsurface sites over on-surface sites is relatively unique. Subsurface hydrogen and oxygen are less stable than on-surface species, and the subsurface sites become occupied only at very high coverage [34]. For hydrogen adsorption on Ni(111), the fcc hollow site is strongly favored over the octahedral sites (by 70 kJ/mol),

and only at high H_2 partial pressures do hydrogen atoms start to diffuse to the subsurface [34]. In addition, for oxygen on Ni(111), we calculated that the fcc hollow sites are preferred over the subsurface octahedral sites by 230 kJ/mol. Carbon's preference for the octahedral subsurface sites can be understood by analyzing the projected density of states. Indeed, the bonding orbitals between the carbon $2p$ orbitals and the Ni $3d$ band shifted from about −4.5 eV for on-surface chemisorption to −6.0 eV for the subsurface octahedral sites, indicative of better orbital overlap.

To determine the location of the bulk carbon atoms, we calculated binding energies for octahedral sites in the second subsurface layer and in the Ni bulk (Table 1). At concentrations corresponding to 0.25 ML, binding energies for the octahedral sites were about 20 kJ/mol weaker in the second subsurface layer than in the first subsurface layer. Binding energy for bulk carbon is a function of carbon concentration. At low concentrations, the binding energy converges to a value similar to that for low concentrations in the second subsurface layer (i.e., about −690 kJ/mol). At high concentrations, the bulk binding energy decreases and becomes weaker than the on-surface binding energy for a C:Ni molar ratio between 1:4 and 1:2. At such high concentrations, the Ni bulk is saturated with carbon, and on-surface chemisorption is preferred. This concentration is consistent with the experimentally observed C:Ni molar ratio of 1:3 for Ni carbide [35]. The bulk lattice constant increases gradually with increasing carbon concentrations from the Ni bulk value of 3.52 Å to a value of 4.08 Å for a C:Ni molar ratio of 1:1.

Based on the data in Table 1, the following model can be proposed. Already at low carbon coverage, on-surface carbon atoms will start to diffuse to the first subsurface layer. Because the binding energy in the first subsurface layer is slightly stronger than the bulk value for similar concentrations, the carbon concentration in the first subsurface layer will gradually build up. At higher concentrations, the subsurface binding energies become weaker, and carbon atoms start to diffuse to the second and third layers to find octahedral sites with higher binding energies. A concentration gradient likely develops, with slightly higher carbon concentrations in the first subsurface layer. At a bulk C:Ni molar ratio of about 1:3, the Ni bulk is saturated with carbon, and carbon atoms start to precipitate to the surface because the low coverage on-surface binding energy becomes stronger than the subsurface and bulk values. Note that this argument is only qualitative, because it neglects the effect of subsurface carbon atoms on the on-surface binding energy. It is likely that a high concentration of bulk carbon lowers the on-surface carbon binding energy or even leads to surface or bulk reconstruction of the Ni catalyst.

Next, we computed the stability of infinite graphene islands on the Ni(111) surface. The lattice constant of graphene of 2.47 Å closely matched the lattice constant of the Ni(111) surface of 2.49 Å, and only a <1% expansion of the graphene lattice is required. Infinite graphene islands correspond to a carbon coverage of 2.0 ML. Four high-symmetry orientations were considered, illustrated in Fig. 2. Based on experimental studies [36,37], two orientations have been proposed for a graphene overlayer on Ni(111). Using extended energy-loss fine-structure spectroscopy, Rosei et al. [36] proposed structure (A), in which one carbon atom is located above the fcc hollow site and another carbon atom is located above the hcp hollow site. Based on low-energy electron diffraction spectroscopy, Gamo et al. [37] proposed structure (B). DFT calculations by Bengaard et al. [22] found that both structures have very similar stability, with structure (A) being 2 kJ/(mol carbon atoms) more stable than structure (B). Our calculations yielded very similar binding energies for all four structures. The most sta-

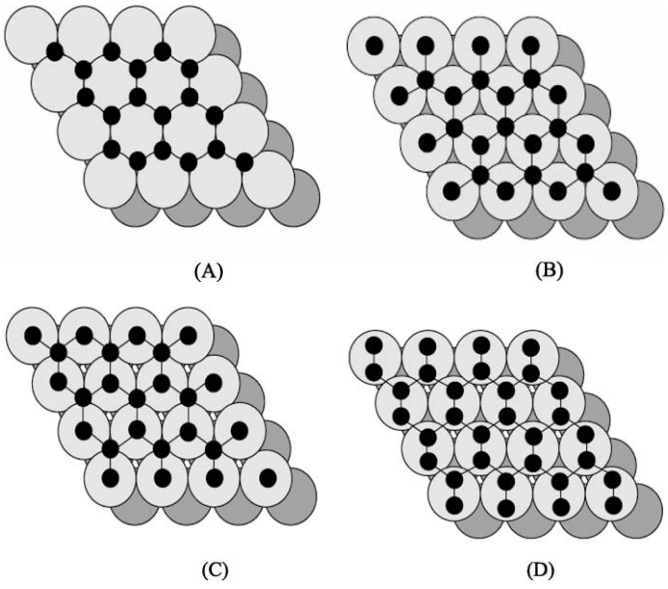

Fig. 2. Possible high symmetry adsorption modes for a graphene overlayer on a Ni(111) surface. Carbon atoms are located at (A) both the fcc and hcp threefold hollow sites; (B) atop and fcc threefold hollow sites; (C) atop and hcp threefold hollow sites; (D) two near atop sites. The small black circles correspond to carbon atoms; the large, light circles correspond to the Ni surface atoms, and the larger, dark circles correspond to Ni atoms in the first subsurface layer.

Table 1
Carbon binding energies for the on-surface hcp hollow sites, the octahedral sites for the first and second subsurface layer and for octahedral sites in the Ni bulk

Site, corresponding coverage or C:Ni molratio	Lattice constant (Å)	Binding energy (kJ/mol)
On-surface hcp hollow site, 0.25 ML	3.52	−662
Octahedral site in first subsurface layer, 0.25 ML	3.52	−707
Octahedral site in second subsurface layer, 0.25 ML	3.52	−686
Octahedral sites in Ni bulk, C:Ni ratio of 1:8	3.64	−686
Octahedral sites in Ni bulk, C:Ni ratio of 1:4	3.74	−669
Octahedral sites in Ni bulk, C:Ni ratio of 1:2	3.86	−644
Octahedral sites in Ni bulk, C:Ni ratio of 1:1	4.08	−550

ble structure (C) had a binding energy of −760 kJ/mol, and the least stable structure (A) had a binding energy of −759 kJ/mol. The C–C bonds provide the main contribution to the carbon binding energy of the graphene islands. The interaction between graphene and the Ni(111) surface is very weak and could not be reliably calculated with DFT. Our calculations yielded a slightly repulsive interaction of 3 kJ/mol, whereas Helveg et al. [38] reported a value of −5 kJ/mol. An analysis of the projected density of states confirms that indeed very little mixing of the Ni 3*d* band and the carbon p_z orbitals occurred. To match the Ni lattice, the graphene lattice constant has to expand slightly from 2.47 to 2.49 Å, causing the slightly positive interaction energy. The calculated distance between the graphene sheet and the Ni(111) surface was 3.3 Å, consistent with an earlier DFT value of 3.2 Å [38] but longer than the experimental value of 2.8 Å [36].

The carbon binding energy for an infinite sheet of graphene is higher than the carbon binding energies for on-surface and subsurface carbon, and graphene is the most stable form of deposited carbon on a Ni(111) surface. This analysis neglects the kinetics of the coking mechanism, however. Indeed, the activation energies for diffusion into the subsurface layer and the energy cost of forming small rather than infinite graphene islands must be considered to complete the picture outlined in this section.

3.2. Kinetics of the formation of bulk carbon and graphene islands from on-surface carbon atoms

Although subsurface carbon is more stable than on-surface carbon, the activation barrier to diffuse from the on-surface fcc hollow site to the octahedral site just below it should not be too high. We performed a series of calculations, summarized in Table 2, to determine the activation barriers for this process. Calculations were performed for a $p(3\times3)$, a $p(2\times2)$, and a $p(1\times1)$ unit cell, corresponding to coverages of 0.11, 0.25, and 1.0 ML, respectively. The calculated barriers depend very strongly on the size of the unit cell. For a $p(1\times1)$ unit cell, a very high barrier of 658 kJ/mol was calculated; for the $p(2\times2)$ unit cell, the barrier decreased to 224 kJ/mol; and for the $p(3\times3)$ unit cell, a low barrier of 68 kJ/mol was calculated. The high barriers for small unit cells can be understood as follows. For carbon atoms to move from the fcc hollow site to the subsurface octahedral site below, they need to move through a triangle of Ni atoms. Going from the reactant state to the transition state, the Ni–Ni distances for that triangle increase, whereas the Ni–Ni distances for the neighboring hollow sites decrease. For a $p(1\times1)$ unit cell, the Ni–Ni distance cannot expand, because there are no neighboring sites to accommodate this expansion. For a $p(3\times3)$ unit cell, the Ni–Ni distance of the triangle increases substantially from 2.49 to 2.95 Å, leading to a much lower barrier. The actual barrier is expected to be even lower than this value, and diffusion from the on-surface to the subsurface sites should be fairly easy. Note that it is indeed not very realistic to assume that all on-surface carbon atoms for a coverage of 1.0 or 0.25 ML diffuse to the subsurface octahedral sites *at the same time*. Based on the temperature at which bulk carbon formation is observed experimentally (500–660 K [18–20]), the barrier must be below about 150 kJ/mol.

We carried out a second set of calculations, also reported in Table 2 and illustrated in Fig. 3, to quantify the effect of on-surface carbon coverage on the activation energies. To limit the computational cost, calculations were done for a $p(2\times2)$ unit cell. Based on the previous results, we expected the calculated barriers to be an overestimation. However, we were interested mainly in the effect of higher carbon coverage on the activation barrier. The lower binding energies at higher surface coverage can be expected to provide a greater driving force for diffusion to the octahedral sites. In the first calculation, one carbon atom was adsorbed at the fcc hollow site of the $p(2\times2)$ unit cell, corresponding to a coverage of 0.25 ML. The barrier to diffuse to the octahedral site is 224 kJ/mol. The final state of this process is shown in Fig. 3A. Next, two carbon atoms were adsorbed at the fcc site hollow sites of a $p(2\times2)$ unit cell, corresponding to a coverage of 0.5 ML. The barrier for one of the two carbon atoms to diffuse to the subsurface site was found to decrease significantly, to 164 kJ/mol. The final state of this process is illustrated in Fig. 3B. In the third calculation, three carbon atoms

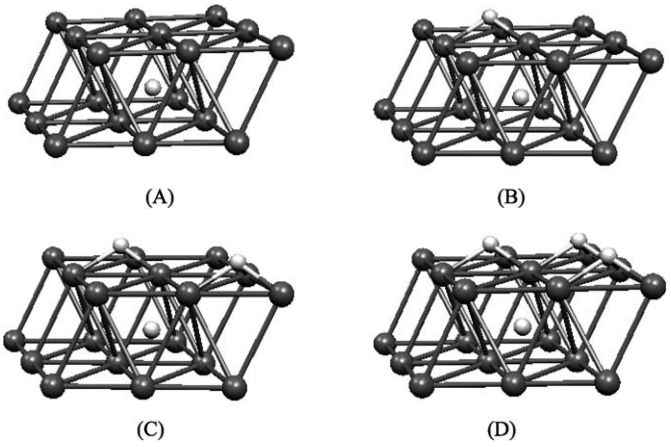

Fig. 3. Product states for the diffusion of one on-surface carbon atom at the fcc hollow site to the octahedral site below for a $p(2\times2)$ unit cell and for coverages of (A) 0.25; (B) 0.5; (C) 0.75; and (D) 1.0 ML.

Table 2
Influence of the unit cell size and of the carbon surface coverage on the activation energy and reaction energy for carbon atom diffusion from the on-surface fcc hollow site to the octahedral site below

	Unit cell			Surface coverage[a] (ML)			
	$p(1\times1)$	$p(2\times2)$	$p(3\times3)$	0.25	0.5	0.75	1.0
Activation energy (kJ/mol)	658	224	68	224	164	138	167
Reaction energy (kJ/mol)	−60	−45	−101	−45	−174	−254	−305

[a] Calculations for a $p(2\times2)$ unit cell. One carbon atom diffuses to the octahedral site. The final states can be found in Fig. 3.

were adsorbed at the fcc hollow sites of the $p(2 \times 2)$ unit cell, corresponding to a coverage of 0.75 ML. Again, the barrier was calculated for one of the three carbon atoms to diffuse to the subsurface octahedral site (Fig. 3C). The barrier further decreased to 138 kJ/mol. Interestingly, the barrier increased to 167 kJ/mol when four carbon atoms were placed at the fcc sites of the $p(2 \times 2)$ unit cell, corresponding to a coverage of 1.0 ML (Fig. 3D). Clearly, two opposing factors affect the calculated barrier. For higher coverages, the repulsion between on-surface carbon atoms increases, leading to a greater driving force for diffusion to the octahedral site. However, higher carbon coverages also increase the energy cost for the expansion of the Ni triangle, because the neighboring hollow sites are occupied as well.

In summary, the barrier for carbon atoms to move from the on-surface to the subsurface sites should not be too high, of the order of 70 kJ/mol. The barrier depends on the surface coverage and decrease with increasing coverage up to about 0.75 ML, but increases again at higher coverage.

Next, we calculated the energy cost to create small graphene islands. The growth of an extended graphene overlayer can be assumed to start with the nucleation of small graphene islands. This picture has also been put forward by Derbyshire and Trimm [39]. The edges of small graphene islands are unsaturated carbon atoms with a lower binding energy than the internal carbon atoms of an extended sheet of graphene. The edge energy is defined as the difference in binding energy between a carbon edge atom and an internal carbon atom in an infinite graphene island. The edge energy is calculated using the two structures shown in Fig. 4. For the single line structure (Fig. 4A), there were two edge and two internal graphene carbon atoms per unit cell, and the edge energy was calculated using

$$E_{\text{edge}} = \frac{E_{(\text{C/Ni})} - E_{(\text{Ni,clean})} - 4E_{\text{graphene}}}{2}, \qquad (2)$$

where $E_{(\text{C/Ni})}$ represents the total energy for the single line structure on the Ni(111) surface, $E_{(\text{Ni,clean})}$ represents the total energy for the clean Ni(111) surface, and E_{graphene} is the total energy per carbon atom for the graphene-covered surface. Using Eq. (2), an edge energy of 151 kJ/mol was calculated for the single line structure. Bengaard et al. [22] reported an edge energy of 172 kJ/mol for the same structure, calculated using the RPBE functional. We also calculated the edge energy for a double-line structure (Fig. 4B). The energy cost to create a carbon edge atom for this structure was 125 kJ/mol. The assumption that the binding energy of the central carbon atoms in structure shown in Fig. 4A is equal to the binding energy of internal carbon atoms in a graphene overlayer is a simplification, leading to an overestimation of the edge energy.

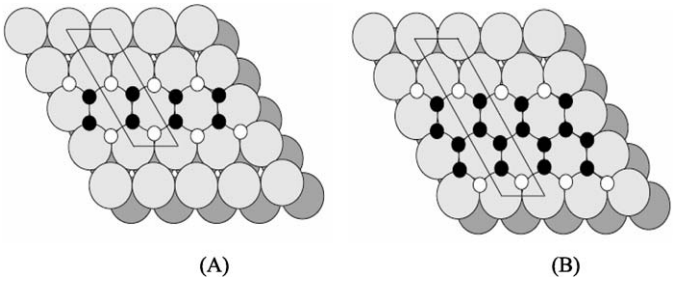

Fig. 4. Model graphene structures used to determine the energy cost for creating small size graphene islands: (A) a single line structure; (B) a double line structure. The white circle indicate unsaturated carbon atoms of the graphene structure, termed edge atoms. The black circles indicate saturated carbon atoms corresponding to internal carbon atoms of graphene. The box illustrates the unit cell used for the calculations.

Using the binding energy for an internal carbon atom of a graphene overlayer of −760 kJ/mol and an edge energy of 125 kJ/mol, we estimated the size of a graphene island that is more stable than isolated carbon atoms at the hcp hollow sites with a binding energy of −660 kJ/mol. Using the hexagonal model shown in Fig. 5, we found that a critical graphene cluster contains about 13 carbon atoms or 3 aromatic rings. For graphene islands with fewer than 13 carbon atoms, the binding energy per carbon atom is weaker than the binding energy for carbon atoms at the hcp hollow sites; for larger graphene islands, the binding energy is stronger. Although this model is a simplification, it illustrates that the formation of a graphene island is a higher-order reaction that requires at least 10–15 carbon atoms to come together. Thus, the formation of a graphene overlayer will be most favorable at high carbon coverage, whereas the formation of subsurface carbon atoms is essentially a first-order reaction.

Several simplifications in the graphene island model should be highlighted. The gray atoms in Fig. 5 are treated as internal graphene carbon atoms, but this overestimates their binding energy; thus, the model probably overestimates the stability of the graphene islands and underestimates the critical size. On the other hand, it has been proposed that graphene grows out of step sites on the Ni catalyst surface [22]. This would reduce the number of edge atoms in small graphene islands and reduce the critical cluster size. In addition, graphene islands grow by the addition of on-surface carbon atoms. The activation energy for this C–C coupling reaction has not been calculated either.

Based on the calculated relative stabilities, the following coking mechanism can be proposed for Ni catalysts (Fig. 6). In a first step, hydrocarbons (C_mH_n) adsorb on the Ni catalyst, and some decompose to form on-surface carbon. Alternatively, CO disproportionates to form on-surface carbon and CO_2. The on-surface carbon atoms can follow three reaction paths. The first option is to react with co-adsorbed hydrogen or oxygen

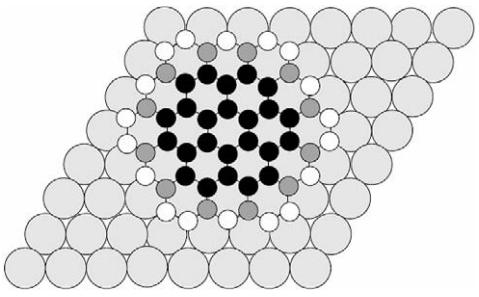

Fig. 5. Model used to calculate the stability of small graphene islands on the Ni(111) surface. Black and grey circles indicate saturated, internal graphene atoms with a carbon binding energy of −760 kJ/mol, white circles indicate unsaturated edge atoms with a carbon binding energy of −635 kJ/mol.

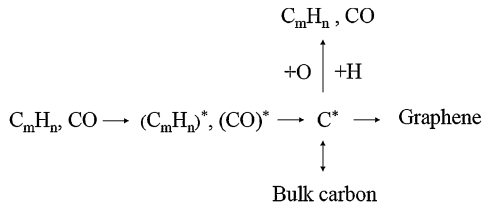

Fig. 6. Proposed mechanism for carbon deposition on Ni-based catalysts. On-surface carbon atoms, C^*, are formed by extensive dehydrogenation of hydrocarbon molecules, C_mH_n, or by CO disproportionation. The on-surface carbon atoms can (i) react with adsorb oxygen and hydrogen to form products, (ii) diffuse to the Ni bulk, or (iii) combine to form graphene islands.

to form products that can possibly desorb. The second option is to diffuse to the octahedral sites of the subsurface layers and to the Ni bulk. This reaction is thermodynamically favored by 50–120 kJ/mol and has a fairly low activation energy of <70 kJ/mol. Diffusion to the bulk continues until a Ni:C molar ratio of about 3:1 is reached. At this point, the bulk is saturated, and carbon atoms accumulate on the surface. The third reaction path leads to the formation of graphene islands. This reaction path is strongly thermodynamically favored, but the formation of initial graphene islands is fairly difficult and seems possible only at high carbon coverages, possibly after the Ni bulk is saturated. Both graphene and bulk carbon are inactive and should be prevented to maximize product yields. In the next section, we propose a method to selectively block the subsurface octahedral sites, thereby forcing the carbon atoms to remain on the surface.

3.3. Effect of subsurface boron atoms on the coking mechanism

As mentioned in the Introduction, Chen et al. [25] have reported that adding boron to Ni catalysts reduces coking during the catalytic partial oxidation of methane while retaining the catalytic activity. Boron is believed to serve as a structural promoter, reducing the average size of the Ni particles to about 8–10 nm. A large reduction in coking has indeed been observed for very small Ni particles (typically <5 nm) [22]. In this section, we use first-principles calculations to provide a possible alternative explanation for the effect of boron on the coking behavior of Ni catalysts.

We begin by discussing the location of the boron promoter. In contrast to the experimental work of Chen et al. [25], we focused mainly on rather low boron concentrations, to minimize the potential effect of boron on the catalytic activity of the Ni catalyst. The binary phase diagram of Ni and B is fairly complex and contains different crystalline phases at higher boron concentrations [40]. The formation of crystalline Ni_3B phases and of a Ni-rich NiB alloy has been reported during the annealing of an amorphous $Ni_{80}B_{20}$ alloy [41]. To avoid the formation of potentially catalytically inactive crystal structures, in the present study we focused on low boron concentrations and retained the bulk fcc structure of Ni.

Similar to carbon chemisorption, we studied boron adsorption at the four high-symmetry sites of the Ni(111) surface for coverages of 0.125–1.0 ML. We also calculated binding

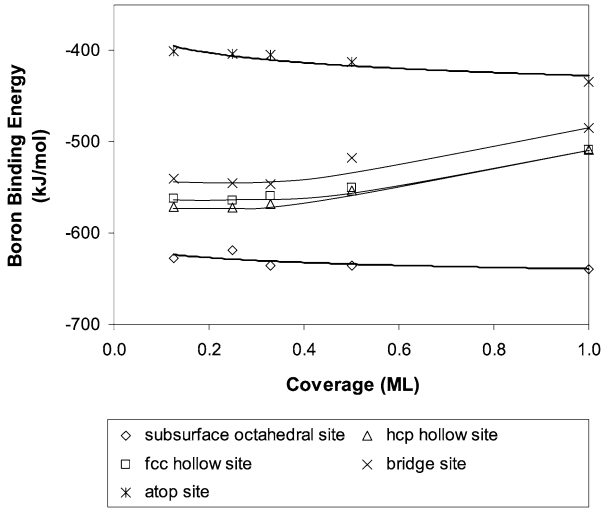

Fig. 7. Boron binding energies for chemisorption at the four high symmetry sites of the Ni(111) surface and at the octahedral sites of the first subsurface layer as a function of coverage. The symbols indicate the calculated binding energies, the lines are guides for the eye.

energies for the octahedral sites of the first subsurface layer. The results, illustrated in Fig. 7, show that the site preference of boron is remarkably similar to that of carbon. Again, the hcp threefold hollow site is the preferred on-surface adsorption site. The boron adsorption energies for the hcp hollow sites are slightly less coverage-dependent than the values for carbon, ranging from −572 kJ/mol for low coverage to −508 kJ/mol for monolayer coverage. The binding energy for the subsurface octahedral sites is remarkably independent of concentration, and it can be expected that all of the octahedral sites of the first subsurface layer will be filled before boron adsorption on the surface becomes favorable. Similar to carbon, the stability of boron in the octahedral sites can be attributed to a strong bonding interaction between boron $2p$ orbitals and the Ni $3d$ band, where the bonding orbitals of octahedral boron are shifted to −4.8 eV, compared with −2.8 eV for boron at the on-surface hcp hollow site.

Next, we calculated binding energies for the second subsurface layer and for bulk octahedral sites (Table 3). Only bulk B:Ni molar ratios below 1:3 were considered, because NiB is known to undergo reconstruction for higher boron concentrations. Binding energies were about 20 kJ/mol weaker for the second subsurface layer than for the first subsurface layer; bulk binding energies were another 20–30 kJ/mol weaker. Binding energies for the first and second subsurface layer were calculated to be stronger than on-surface binding energies. Bulk values were similar to on-surface values for low coverages. From these values, it seems that boron fills the octahedral sites in a layer-by-layer fashion; the octahedral sites of the first subsurface layer are completely filled before occupation of the octahedral sites of the second and third subsurface layer begins. Adsorption in the bulk seems less likely, because the binding energies are weaker than the low-coverage on-surface binding energies. To test this concept of layer-by-layer diffusion, we calculated the total binding energy for a number of configurations for four boron atoms in a $p(2 \times 2)$ unit cell (Table 4).

Table 3
Boron binding energies for the on-surface hcp hollow sites, the octahedral sites for the first and second subsurface layer and for octahedral sites in the Ni bulk

Site, corresponding coverage or B:Ni molratio	Lattice constant (Å)	Binding energy (kJ/mol)
On-surface hcp hollow site, 0.25 ML	3.52	−572
Octahedral site in first subsurface layer, 0.25 ML	3.52	−620
Octahedral site in second subsurface layer, 0.25 ML	3.52	−600
Octahedral sites in Ni bulk, B:Ni ratio of 1:8	3.66	−570
Octahedral sites in Ni bulk, B:Ni ratio of 1:4	3.79	−581

Table 4
Boron binding energies for different configurations of four boron atoms in a $p(2 \times 2)$ unit cell

Location of the boron atoms[a]	Binding energy (kJ/mol)
4 in the first subsurface layer	−636
3 in the first subsurface layer, 1 in the second	−630
2 in the first subsurface layer, 2 in the second	−616
3 in the first subsurface layer, 1 at the on-surface fcc site	−612
2 in the first subsurface layer, 2 at the on-surface fcc sites	−578
1 in the first subsurface layer, 3 at the on-surface fcc sites	−545

[a] If multiple configuration are available, only the most stable binding energy is reported.

Three adsorption sites were considered: on-surface fcc hollow sites and octahedral sites in the first and second subsurface layers. Again, the preference for the octahedral sites in the first subsurface layer was confirmed. Hence, adding a small amount of boron to partially or fully occupy the octahedral sites of the first subsurface layer might be sufficient to significantly affect catalyst behavior. In addition to chemisorption at the bulk octahedral sites, a substitutional NiB alloy was considered; however, this structure was found to be about 20 kJ/mol less stable than adsorption at the octahedral sites, and thus it was not considered further.

Because boron atoms strongly prefer the octahedral sites of the first subsurface layer, they might effectively block these sites for carbon and force carbon atoms to remain on the catalyst surface, available for reaction. This method to prevent coking differs from the mechanism proposed for such promoters as potassium, sulfur, and gold, which selectively block the step sites to suppress the formation of graphene [22]. To gain insight into the effect of boron on carbon deposition, we performed various calculations. First, we investigated whether carbon atoms can force boron atoms located in the first subsurface layer to the surface. The energy was calculated for the two model structures shown in Fig. 8. It was found that the combination of one on-surface carbon atom and four boron atoms in the first subsurface layer (Fig. 8A) is 118 kJ/mol more stable than the combination of the carbon atom in the first subsurface layer and the boron atom on-surface (Fig. 8B). We propose that the subsurface boron atoms can effectively prevent carbon atoms from diffusing to the bulk and force the carbon atoms to remain on the surface.

In addition, the boron promoter might influence the on-surface carbon binding energy. Besenbacher et al. [9] suggested that the binding energy of a surface carbon atom can indicate the atom's tendency to form a graphene overlayer. Indeed, as suggested in Section 3.2, the nucleation of graphene islands may be very sensitive to the carbon coverage and thus may depend on the carbon binding energy. We calculated carbon

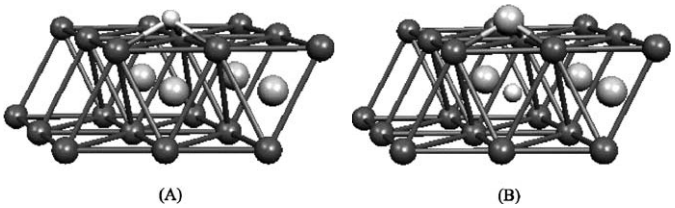

Fig. 8. Structures to study the stability of a carbon atom on a boron promoted Ni(111) surface. (A) Structure with one on-surface carbon atom and four subsurface boron atoms (B) structure with one carbon atom and three boron atoms in the octahedral sites of the first subsurface layer and one on-surface boron atom. The large grey balls indicate boron atoms, the small grey ball indicates the carbon atom and the black balls indicate Ni atoms.

binding energies for a surface with all octahedral sites of the first subsurface layer occupied by boron atoms and found that these carbon binding energies decreased by about 120 kJ/mol for a carbon coverage of 0.25 ML (Table 5, column 6). Interestingly, the preferred adsorption site changed from the hcp threefold-hollow site to the fcc site above a boron atom. Hence putting boron atoms in all octahedral sites of the first subsurface layer not only prevents the formation of bulk carbon, but also may reduce the nucleation of graphene islands.

Creating a catalyst where *all* octahedral sites of the first subsurface layer are occupied by boron atoms might be technically challenging. The question arises as to whether octahedral sites without a boron atom provide pathways for carbon atoms to diffuse into the bulk. To test this possibility, we calculated carbon binding energies for a 0.25-ML coverage on a surface with 25, 50, and 75% of the octahedral sites in the first subsurface layer occupied by boron atoms. The calculations are illustrated in Fig. 9, and the results are presented in Table 5. We found that even in the presence of a single octahedral vacancy, the carbon atom prefers to remain on the surface rather than diffuse to the vacant octahedral site. The carbon binding energy at the available octahedral site is 37 kJ/mol weaker than at the fcc hollow site above it. However, when the number of octahedral vacancies was increased further, carbon atoms be-

Table 5
Effect of the concentration of boron atoms in the octahedral sites of the first subsurface layer on the carbon binding energies at the hollow and octahedral sites

Carbon binding site	Boron concentration (%)				
	0	25	50	75	100
Octahedral site of the first subsurface layer (4[a])	−707	−711	−609	−563	n.a.
Fcc hollow site above a boron atom (3[a])	n.a.	−676	−576	−561	−544
Fcc hollow site (2[a])	−655	−676	−590	−600	n.a.
Hcp hollow site (1[a])	−662	−665	−567	−571	−531

[a] Corresponding site in Fig. 9.

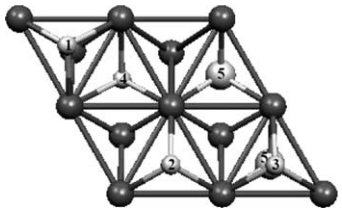

Fig. 9. Illustration of the adsorption sites for a Ni(111) surface with boron atoms located in the octahedral sites of the first subsurface layer. (1) hcp threefold hollow site; (2) fcc threefold hollow site; (3) fcc threefold hollow site above a boron atom; (4) carbon atom occupying the octahedral site; (5) boron atom occupying the octahedral site. The large grey balls indicate the boron atoms, the small grey balls indicate the carbon atoms and the large black balls indicate the Ni atoms.

gan to occupy these vacancies and began to diffuse to the Ni bulk.

4. Conclusions

We performed ab initio DFT calculations to gain insight into the mechanism of carbon deposition on Ni catalysts. Based on our analysis, we propose using boron as a promoter to reduce the deactivation of Ni-based catalysts by coking. The relative stability of three types of chemisorbed carbon—on-surface chemisorbed carbon, bulk carbon, and extended graphene islands—was calculated. On-surface carbon atoms were found to be relatively unstable. Diffusion to octahedral sites of the first subsurface layer is thermodynamically preferred by 50–120 kJ/mol, and the corresponding activation energy is only about 70 kJ/mol. Extended graphene islands are even more stable than bulk carbon, by about 60 kJ/mol. However, the nucleation of graphene islands is rather difficult and may require relatively high carbon coverage.

Ab initio calculations indicate that boron atoms prefer to adsorb in the octahedral sites of the first subsurface layer. We propose that these boron atoms effectively block the subsurface sites and prevent carbon diffusion into the bulk, forcing carbon atoms to remain on the surface, available for reaction. In addition, the boron promoter in the first subsurface layer reduces the on-surface carbon binding energy and thus may reduce carbon coverage, which in turn could decrease the nucleation rate of graphene islands.

Acknowledgment

The authors thank Dr. James Highfield for interesting discussions on the experimental aspects of boron promotion.

References

[1] M.V. Twigg, Catalyst Handbook, second ed., Manson Pub., London, 1996.
[2] V. Ponec, G.C. Bond, Catalysis by Metals and Alloys, Elsevier, New York, 1995.
[3] M.C. Zonnevylle, J.J.C. Geerlings, R.A. van Santen, Surf. Sci. 240 (1990) 253.
[4] R.W. Joyner, G.R. Darling, J.B. Pendry, Surf. Sci. 205 (1988) 513.
[5] R. Hughes, Deactivation of Catalysis, Academic Press, San Diego, 1984.
[6] J.R. Rostrup-Nielsen, P.e. Højlund Nielsen, in: J. Oudar, H. Wise (Eds.), Deactivation and Poisoning of Catalysts, Dekker, New York, 1985.
[7] M. Yudasaka, R. Kikuchi, T. Matsui, Y. Ohki, S. Yoshimura, E. Ota, Appl. Phys. Lett. 67 (1995) 2477.
[8] J.R. Rostrup-Nielsen, J.H.B. Hansen, J. Catal. 144 (1993) 38.
[9] F. Besenbacher, I. Chorkendorff, B.S. Clausen, B. Hammer, A.M. Molenbroek, J.K. Nørskov, I. Stensgaard, Science 279 (1998) 1913.
[10] J.R. Rostrup-Nielsen, J. Catal. 85 (1984) 31.
[11] J. Rostrup-Nielsen, D.L. Trimm, J. Catal. 48 (1977) 155.
[12] S.C. Tsang, J.B. Claridge, M.L.H. Green, Catal. Today 23 (1995) 3.
[13] L.F. Albright, J.C. Marek, Ind. Eng. Chem. Res. 27 (5) (1988) 755.
[14] M. Pérez-Cabero, E. Romeo, C. Royo, A. Monzón, A. Guerrero-Ruíz, I. Rodríguez-Ramos, J. Catal. 224 (2004) 197.
[15] J.-W. Snoeck, G.F. Froment, M. Fowles, J. Catal. 169 (1997) 240.
[16] J.-W. Snoeck, G.F. Froment, M. Fowles, J. Catal. 169 (1997) 250.
[17] F. Abild-Pedersen, J.K. Nørskov, J.R. Rostrup-Nielsen, J. Sehested, S. Helveg, Phys. Rev. B 73 (2006) 115419.
[18] J. Nakamura, H. Hirano, M. Xie, I. Matsuo, T. Yamada, K.-I. Tanaka, Surf. Sci. 222 (1989) L809.
[19] H. Nakano, S. Kawakami, T. Fujitani, J. Nakamura, Surf. Sci. 454 (2000) 295.
[20] F.C. Schouten, O.L.J. Gijzeman, G.A. Bootsma, Surf. Sci. 87 (1979) 1.
[21] E. Bjørgum, D. Chen, M.G. Bakken, K.O. Christensen, A. Holmen, O. Lytken, I. Chorkendorff, J. Phys. Chem. B 109 (2005) 2360.
[22] H.S. Bengaard, J.K. Nørskov, J. Sehested, B.S. Clausen, L.P. Nielsen, A.M. Molenbroek, J.R. Rostrup-Nielsen, J. Catal. 209 (2002) 365.
[23] D.J. Klinke II, S. Wilke, L.J. Broadbelt, J. Catal. 178 (1998) 540.
[24] N.T. Andersen, F. Topsøe, I. Alstrup, J.R. Rostrup-Nielsen, J. Catal. 104 (1987) 454.
[25] L. Chen, Y. Lu, Q. Hong, J. Lin, F.M. Dautzenberg, Appl. Catal. A 292 (2005) 295.
[26] J. Li, G. Jacobs, Y. Zhang, T. Das, B.H. Davis, Appl. Catal. A 223 (2002) 195.
[27] J.P. Perdew, J.A. Chevary, S.H. Vosko, K.A. Jackson, M.R. Pedersen, D.J. Singh, C. Fiolhais, Phys. Rev. B 46 (1992) 6671.
[28] (a) G. Kresse, J. Hafner, Phys. Rev. B 47 (1993) 558;
(b) G. Kresse, J. Hafner, Phys. Rev. B 49 (1994) 14,251.
[29] (a) G. Kresse, J. Furthmüller, Phys. Rev. B 54 (1996) 11,169;
(b) G. Kresse, J. Furthmüller, Comput. Mater. Sci. 6 (1996) 15.
[30] P.E. Blöchl, Phys. Rev. B 50 (1994) 17,953.
[31] G. Kresse, D. Joubert, Phys. Rev. B 59 (1999) 1758.
[32] D.R. Lide (Ed.), CRC Handbook of Chemistry and Physics, 79th ed., CRC Press, Boca Raton, FL, 1998.
[33] I. Alstrup, J. Catal. 109 (1988) 241.
[34] J. Greeley, W.P. Krekelberg, M. Mavrikakis, Angew. Chem. Int. Ed. 43 (2004) 4296.

[35] P. Hooker, B.J. Tan, K.J. Klabunde, S. Suib, Chem. Mater. 3 (5) (1991) 947.
[36] R. Rosei, M. De Crescenzi, F. Sette, C. Quaresima, A. Savoia, P. Perfetti, Phys. Rev. B 28 (1983) 1161.
[37] Y. Gamo, A. Nagashima, M. Wakabayashi, M. Terai, C. Oshima, Surf. Sci. 374 (1997) 61.
[38] S. Helveg, C. López-Cartes, J. Sehested, P.L. Hansen, B.S. Clausen, J.R. Rostrup-Nielsen, F. Abild-Pedersen, J.K. Nørskov, Nature 427 (2004) 426.
[39] F.J. Derbyshire, D.L. Trimm, Carbon 13 (1975) 189.
[40] O. Teppo, P. Taskinen, Mater. Sci. Technol. 9 (3) (1993) 205.
[41] J.M. Riveiro, P. Muñiz, J.P. Andres, M.A. Lopez de la Torre, J. Magn. Magn. Mater. 188 (1998) 153.